Exploiting CO2Derived Carbon in LithiumIon Batteries

ADVANCED ENERGY & SUSTAINABILITY RESEARCH
www.advenergysustres.com

Exploiting CO_2-Derived Carbon in Lithium-Ion Batteries

Nicolò Albanelli, Alessandro Gregucci, Shoayb Mojtahedi, Antunes Staffolani, Sander Ratso, Einar Karu, Sebastian Pohlmann, Catia Arbizzani,* and Francesca Soavi*

The extraction of valuable carbon-based products from CO_2 reduction represents a promising route to reduce greenhouse gas emissions, promote circular economy practices, and facilitate the integration of energy storage sources such as Li-ion batteries (LIBs). Using such extremely valuable sustainable products obtained from the CO_2 capture process can solve not only the global warming problems but also the high demand of the battery industry to provide graphite and highly conductive additives. Herein, a carbon nanomaterial (CNM) extracted from CO_2 reduction treatment is used as the conductive additive in LIB graphite anode and lithium iron phosphate cathode. The electrodes are produced by casting, using both the conventional poly(vinylidene fluoride) binder, dissolved in N-methyl-2-pyrrolidone, and sodium alginate as a green, water-soluble, alternative binder. The electrochemical performance of the CNM-based electrodes is here compared to that of LIB cathodes and anodes produced with a commercial carbon additive. The electrodes featuring CNM offer electrochemical performance close to those of conventional electrodes in which commercial conductive additives are utilized.

1. Introduction

In the past 20 years, climate change has posed a threat not only to mankind, but also to the environment and all the other livings things. Indeed, several drastic phenomena are already occurring such as the increase of the average temperature of seas surface,[1,2] desertification,[3,4] extreme weather events,[5] and permafrost melting.[6] These events are likely due to global warming triggered by the emission of greenhouse gases (GHGs) such as CO_2 and CH_4.[7] In a rough estimation, ≈70% of GHGs are produced by the burning of fossil fuels (coal and natural gas mostly) for electrical energy production and transport (burning of gasoline and Diesel).[8,9] Renewable energy sources and CO_2 capture technologies can mitigate the effects of global warming. However, due to the intermittent nature of the former, energy storage systems (ESS) are needed. Another solution, which will be employed simultaneously, is the electrification of transport systems such as in hybrid electric vehicles and battery electric vehicles. Several devices are available for energy storage; however, among them, lithium-ion batteries (LIBs) are the ESS of choice and market leader thanks to their high energy density, high energy efficiency, long cycle life (especially in the case of lithium iron phosphate-based batteries), and possibility to design modular systems from mWh up to kWh of storage.[10] Nevertheless, their future massive use in both transport and stationary application is still hindered by aspects such as safety, energy density, energy efficiency, and charging speed. These features are strictly dependent on the materials used inside LIBs, and every component must be not only optimized in terms of performance, but also in terms of recyclability and especially sustainability. LIBs electrodes are usually made of an active material, which is the component that reversibly stores charge, a polymer binder used to hold together all the components to the current collector, and a carbon black (CB), which is needed to ensure a proper electron-conductive network. CB is commonly produced from the partial combustion of heavy petroleum products such as tar from fluid catalytic cracking, coal

N. Albanelli, A. Gregucci, S. Mojtahedi, A. Staffolani, C. Arbizzani, F. Soavi
Department of Chemistry "Giacomo Ciamician"
Alma Mater Studiorum University of Bologna
Via P. Gobetti 85, 40129 Bologna, Italy
E-mail: antunes.staffolani@unibo.it; catia.arbizzani@unibo.it

A. Gregucci, S. Mojtahedi
Department of Applied Science and Technology (DISAT)
Politecnico di Torino
C.so Duca degli Abruzzi 24, 10129 Torino, Italy

The ORCID identification number(s) for the author(s) of this article can be found under https://doi.org/10.1002/aesr.202400217.

DOI: 10.1002/aesr.202400217

A. Staffolani, C. Arbizzani, F. Soavi
National Reference Center for Electrochemical Energy Storage (GISEL)—INSTM
Via G. Giusti 9, 50121 Firenze, Italy

A. Staffolani, F. Soavi
ENERCube
Centro di Ricerca Ambiente, Energia e Mare
Centro di Ricerca Interdisciplinare Fonti Rinnovabili, Ambiente, Mare ed Energia (CIRI-FRAME)
Alma Mater Studiorum University of Bologna
Viale C. Menotti 48, 48121 Marina di Ravenna, Italy

S. Ratso
National Institute of Chemical Physics and Biophysics
Akadeemia tee 23, 12618 Tallinn, Estonia

S. Ratso, E. Karu, S. Pohlmann
UP Catalyst OÜ
Akadeemia tee 23, 12618 Tallinn, Estonia

tar, and, in small amounts, vegetable oils. For this reason, even though CB is present in a small percentage in LIBs, its presence can affect the sustainability of the device. Indeed, as reported in the Compilation of Air Pollutant Emissions Factors from the U.S. Environmental Protection Agency, the production of CB can lead to the emission of a series of gaseous pollutants such as carbon oxides, nitrogen oxides, sulfur oxides, methane, hydrogen sulfide, and other volatile organic compounds.[11] Furthermore, as reported in the lifecycle assessment studies,[12–14] the production of 1 kg of CB can lead to the formation of ≈2.4 kg of CO_2 equivalents. For this reason, to ensure the complete environmental sustainability of LIBs, even CB must be replaced with a greener alternative. A valid substitute can be carbon nanomaterials (CNMs) prepared from electrolysis of CO_2 in molten carbonates.[15,16] In contrast to the production of CB from fossil fuels, these CNM are prepared by consuming CO_2 rather than emitting it. CO_2 is stored in the stable form of elemental carbon. Faradaic efficiencies of >95% and current densities >2 A cm^{-2} have been demonstrated for the electrosynthesis of carbon from molten carbonates,[17,18] with ≈100% selectivity at <800 °C (competing aqueous technologies for CO_2 electrolysis struggle to reach selectivity >90% and current densities >150 mA cm^{-2}[19,20]). Coupling this efficiency with renewable energy can lead to 0.890–0.971 kg of captured CO_2 per kg of carbon produced depending on the energy source (thus a CO_2 equivalent from –0.89 to –0.971[21]). Furthermore, the CNM produced in this way are orders of magnitude cheaper than carbon nanotubes,[22] which are commonly prepared by chemical vapor deposition.[23,24]

In addition, conventional LIB electrode manufacturing exploits a fluorinated binder, like poly(vinylidene difluoride) (PVdF) which needs N-methyl-2-pyrrolidone (NMP) as solvent/dispersant, both very toxic for humans and the environment.[25] This process needs expensive and a high-energy demanding atmosphere-controlled environment. In addition, the presence of PVdF can be critical in the management of spent LIBs, that during the traditional incineration might generate volatile and toxic organofluorine compounds.[26–28] Hence, the use of water-soluble binders is considered a practical solution to alleviate negative environmental impact of LIB electrode production, related to the use of PVdF-NMP. Different natural polymers have already been reported as viable alternatives to PVdF, and carboxymethyl cellulose is already used as an electrode binder in marketed LIBs.[29–32] In turn, other natural polymers like Na-alginate or Pullulan have been demonstrated as valuable binder alternatives to PVdF.[30–32]

In this work, the substitution of CB in LIB electrodes with the greener alternative of CNMs produced from CO_2 electrolysis in molten carbonates is reported. Negative and positive electrodes were prepared with graphite and $LiFePO_4$ (LFP) as active materials, respectively, and CNM as conductive additive. Benchmark electrodes were prepared with CB instead of CNM as carbon additive. The positive and negative electrodes were prepared by both water-processable and NMP-processable formulations, with Na-alginate and polyvinylidene difluoride as binder, respectively. The viability of the use of CNMs in water-processed electrodes is demonstrated by half-cell electrochemical tests complemented by several structural, morphological, and surface analyses, like scanning electron microscopy (SEM), transmission electron microscopy (TEM), X-ray diffraction, and N_2 physisorption.

2. Experimental Section

2.1. Materials

All reagents were used as received and without any purification.

Graphite SFG44, C-NERGY SUPER C65, and SUPER C45 were purchased from Imerys S.A. (43 Quai de Grenelle, 75 015 Paris) and used as received. LFP-NCO (nanosize cocrystalline olivine) was purchased from Advanced Lithium Electrochemistry Co., Ltd (Singhua Rd., Taoyuan City, Taiwan). PVdF HSV 900 was purchased from Arkema srl (Via Caldera, 21 20153 Milano - Italia). Na-alginate (Na-Alg, sodium salt from brown algae) and N-methyl-2-pyrrolidone (NMP, ReagentPlus 99%) were purchased from Merck (Via Casilina 125 Roma, 00176, Italy). LP30 electrolyte (1M $LiPF_6$ in ethylene carbonate:dimethyl carbonate, 1:1 vol%) was purchased from Solvionic (11 Chemin des Silos, 31100 Toulouse, France). The CNM produced by UP Catalyst CATASOL was a commercial product and it was used as received.

2.2. Synthesis of Carbon Nanomaterial

CNM were produced by a proprietary electrochemical process by UP Catalyst CATASOL. Briefly, solid Li_2CO_3 and a metal catalyst with a known ratio was mixed well and heated and dried to remove residual moisture. The mixture was then heated to beyond its melting point and electrodes were inserted into the molten carbonate. The electrodes consisted of a nickel–chromium anode and a Zn–steel cathode. The CO_3^{2-} anions in the molten electrolyte are in equilibrium with CO_2 in the surrounding environment according to the following equations.

$$CO_{3(l)}^{2-} \rightleftarrows CO_{2(g)} + O^{2-} \quad (1)$$

$$CO_{2(g)} + CO_{3(l)}^{2-} \rightleftarrows C_2O_{5(l)}^{2-} \quad (2)$$

As the potentiostatic electrolysis began, the carbon center in the CO_3^{2-} anions was reduced to elemental C according to a four-electron cathodic reaction here reported (Equation (3)).[33,34]

$$CO_3^{2-} + 4e^- \rightleftarrows C + 3O^{2-} \quad (3)$$

The anodic reaction for the molten salt electrolyzer is oxygen evolution (Equation (4)).

$$2O^{2-} \rightleftarrows O_2 + 4e^- \quad (4)$$

which brings the following full cell reaction (Equation (5))

$$CO_2 \rightleftarrows C + O_2 \quad (5)$$

After potentiostatic electrolysis between two metal electrodes, the electrodes were removed from the electrolyte and the solid product was scraped off the cathode. This synthesis process had a Faradaic efficiency of >85%.[33] This product was then purified of electrolyte residue and accessible catalyst particles using an aqueous HCl solution. After this, the solid carbon product was filtered and dried.

2.3. Structural and Morphological Characterization

Diffractograms were collected by a PANalytical X'Pert PRO powder diffractometer equipped with a X'Celerator detector, a CuKα radiation ($\lambda = 1.5406$ Å, 40 mA, 40 kV) radiation source, and a Ni filter by continuous scanning mode (step 0.017° 2θ step size, 10 s/step scan rate). TEM micrographs of CNM were acquired using a Philips TEM CM100 with an acceleration voltage of 80 kV. SEM on the CNM-based electrodes was performed using a Leica/Cambridge Stereoscan 360. The physisorption measurements were performed with a Tristar II Plus physisorption meter. After degassing, the surface area (SA) of the CNM was measured with both CO_2 and N_2 as adsorbed gases at the temperatures of $T = 273.15$ K and $T = 77$ K, respectively. In the case of the measurement performed with CO_2, the analysis truncated around 0.03 due to CO_2 saturation pressure being 26 000 mm Hg, making Brunauer-Emmett-Teller (BET) unreliable.

Thus, the SA was then calculated using the Dubinin–Radushkevich method.[35] Each measurement was performed with three replicates.

2.4. Electrode Processing

First, the binder was dissolved in its solvent (H_2O for Na-Alginate and NMP for PVdF) and stirred for 2 h. Afterward, the binder solution was transferred into the mixer (Ultraturrax Tube Drive and vacuum mixer for LFP and graphite, respectively), along with the active materials (NCO-LFP or graphite SFG44), and mixed for 30 min. Then, the conductive additive (CNM or CB) was added to the slurry mixture and left stirred for 1 h. The electrode formulations (active material: conductive additive: binder) are reported in **Table 1**. The electrode slurries were cast on their respective current collectors (10 μm Cu and 20 μm Al for anode and cathode, respectively), with a wet thickness of 300 μm. The casting procedure was performed with a mini coating machine (Hohsen Corporation, Osaka, Japan) at 10 mm s^{-1}. After casting, the electrode layers were dried at 80 °C in a thermostatic oven for 3 h. Electrode with a diameter Ø = 9 mm were then punched, pressed at 3.1 ton cm^{-2}, and weighed. Electrodes were then dried under vacuum with a Büchi glass oven (Büchi B-585, BÜCHI Labortechnik AG, Meierseggstrasse 40, Postfach, 9230 Flawil, Switzerland) at 80 and 120 °C for Na–Alg-based and PVdF-based electrodes, respectively. The prepaer electrode layers and their formulation are summarized in Table 1.

2.5. Electrochemical Characterization

Three-electrode PTFE cells (BOLA, Bohlender GmbH, Grünsfeld, Germany) were used for the electrochemical characterization. The prepared electrodes were used as working electrodes, while Li metal with a diameter of Ø = 10 mm was used for both the reference and the counter electrodes. Whatman GF/A glass fiber discs with a diameter of Ø = 10 mm were used as separators, and they were soaked with LP30 electrolyte solution. The electrochemical characterization includes cyclic voltammetry (CV), galvanostatic cycling, and rate capability. CV were performed in the potential windows 0.02 V/1.5 V versus Li^+/Li and 2.5 V/4.0 V versus Li^+/Li for graphite and LFP, respectively, with a scan rate of 200 μV s^{-1}. Stability tests were performed using galvanostatic cycling at 1C rate (372 and 170 mA g^{-1} for graphite and LFP, respectively) in the same potential window used for CV tests. In the case of the graphite electrodes, a constant current–constant voltage (CC–CV) protocol was used in the galvanostatic tests. Namely, a constant voltage period was applied after the galvanostatic charge with a potential hold at 0.02 V versus Li^+/Li until the current dropped to C/70 (5.3 mA g^{-1}), with a time limit of 30 min. Rate capability test protocols are reported in **Table 2**.

All the electrochemical analyses were performed with VMP and VSP galvanostat/potentiostat from Bio-Logic (BioLogic, 4 rue Vaucanson, 38170 Seyssinet-Pariset, France). All the cell assembly procedures were performed in a LabMaster SP MBraun Ar-filled glovebox with $H_2O < 0.1$ ppm, and $O_2 < 0.1$ ppm (M. BRAUN INERTGAS-SYSTEME GMBH, Dieselstr. 31, D-85748 Garching, Germany).

All the specific capacity values shown in this article are referred to the sole mass of the active material. If not stated, the potential values were always referred to the Li redox couple Li^+/Li.

3. Results and Discussion

3.1. Structural and Morphological Characterization of CNM and CNM-Based Electrodes

Figure 1 reports the results of the structural and morphological characterization of CNM. As shown by the TEM images reported in Figure 1a,b, CNM is made by distorted rods with a diameter of ≈100 nm. The rods length is not homogeneous and, thus, it was

Table 1. Electrode layers prepared in this work and their formulation.

Name	Active material/%	Carbon additive/%	Binder/%	Solvent	Average active material loading [mg cm^{-2}]
G_PVdF_CNM	Graphite SFG44/90%	CNM/5%	PVdF/5%	NMP	≈5
G_PVdF_CB	Graphite SFG44/90%	SUPER C65/5%	PVdF/5%	NMP	≈5
G_Alg_CNM	Graphite SFG44/90%	CNM/5%	Na-Alg/5%	H_2O	≈5
G_Alg_CB	Graphite SFG44/90%	SUPER C65/5%	Na-Alg/5%	H_2O	≈3
LFP_PVdF_CNM	NCO-LFP/80%	CNM/10%	PVdF/10%	NMP	≈6
LFP_PVdF_CB	NCO-LFP/80%	SUPER C65/10%	PVdF/10%	NMP	≈4
LFP_Alg_CNM	NCO-LFP/80%	CNM/10%	Na-Alg/10%	H_2O	≈2
LFP_Alg_CB	NCO-LFP/80%	SUPER C65/10%	Na-Alg/10%	H_2O	≈2

Table 2. Rate capability test protocols used in this work.

Electrode	Protocol					
LFP-based electrodes	4 cycles at C/10 (17 mA g^{-1})	4 cycles at C/5 (34 mA g^{-1})	4 cycles at C/2 (85 mA g^{-1})	4 cycles at 1C (170 mA g^{-1})	3 cycles at C/5 (34 mA g^{-1})	–
Graphite-based electrodes	3 cycles at C/20 (18.6 mA g^{-1})	3 cycles at C/ 10(37.2 mA g^{-1})	3 cycles at C/ 5(74.4 mA g^{-1})	3 cycles at C/2 (186 mA g^{-1})	3 cycles at 1C (372 mA g^{-1})	3 cycles at C/5 (74.4 mA g^{-1})

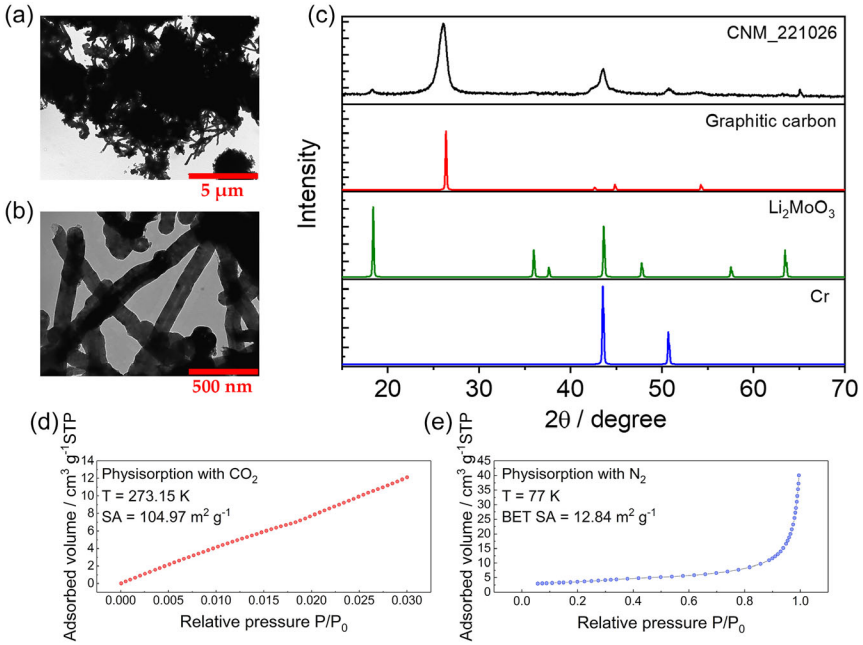

Figure 1. a,b) TEM micrographs of CNM. (a,b) Scale bar of 5 µm and 500 nm, respectively. c) X-ray diffractogram of the synthesized CNM, graphitic carbon (red line, PDF#41-1487), Li_2MoO_3 (green line, PDF#88-0303), and Cr (blue line, PDF# 65-3316). d) CO_2 and e) N_2 physisorption curves of CNM, with the corresponding calculated SA.

not possible to calculate the aspect ratio of the rods. The X-ray diffractogram of CNM is reported in Figure 1c. The reflection pattern agrees with the reference diffractogram of graphitic carbon (also reported in Figure 1c for a comparison) with broadened reflexes, probably due to the presence of a large fraction of amorphous carbon. The small reflexes at ≈19° and 43° can be assigned to the phase Li_2MoO_3, while the signal at 51° to Cr. The presence of foreign species such as Li_2MoO_3 and Cr can be explained by the partial leaching of the electrode material during the synthesis of CNM.[16]

Physisorption tests of CO_2 and N_2 were carried out for the evaluation of the CNM SA. The related isotherms along with the calculated SAs are reported Figure 1c,d. The CNM surface area is 104.97 and 12.84 $m^2 g^{-1}$ when measured with CO_2 and N_2, respectively. Notably, SA evaluated by N_2 adsorption is lower than that of the commercially available CB Super C65 (61.61 $m^2 g^{-1}$) and Super C45 (45.99 $m^2 g^{-1}$).[36]

Figure 2 reports the SEM images of the CNM-based electrodes. Specifically, Figures 2a,b and c,d show the images of PVdF- and Na–Alg-based LFP electrodes. Figure 2e,f and g,h reports the SEM images of PVdF- and Na–Alg-based graphite electrodes, respectively. Figure 2a–d show that LFP is characterized by spherical-shaped particles with submicrometer diameter. In both PVdF and Na–Alg based electrodes, is not possible to detect the CNM additive. This is probably due to the low percentage of CNM present in the composite layer with respect to the other electrode components, and the smaller CNM size compared to the LFP particles. Breaking of the CNM rods during the grounding/mixing phase cannot be excluded.

In the case of the negative electrodes (Figure 2e–h), the graphite particles are characterized by flake-like morphology with a size of ≈30–40 µm. As in the case of the LFP, it is not possible to discern where the CNM additive is located, probably due to the same reason explained above. However, in all the prepared electrodes, it was possible to assess a good dispersion of the active materials. Notably, no significative difference in the electrode morphology can be appreciated when PVdF or Na–Alg binder is used.

3.2. Electrochemical Comparison of CNM- and CB-Containing Electrodes

3.2.1. Characterization of LFP-Based Electrodes

Figure 3 reports the main results of the voltammetric and galvanostatic characterization of LFP electrodes produced with PVdF

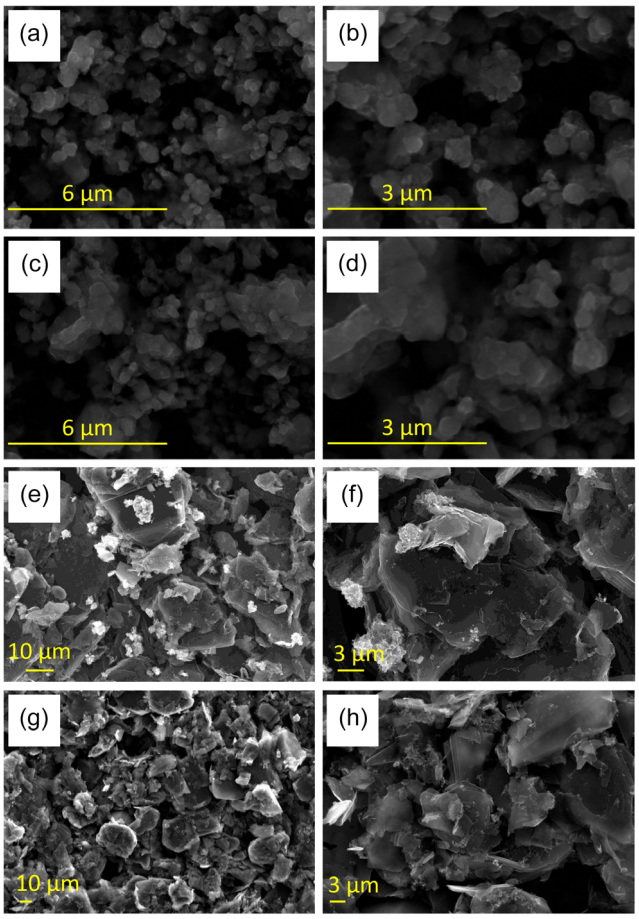

Figure 2. SEM micrographs of a,b) PVdF- and c,d) Na–Alg-based LFP electrodes, and of e,f) PVdF- and g,h) Na–Alg-based graphite electrodes.

and CNM or CB. In Figure 3a, the 1st and 4th CV cycles of LFP_PVdF_CNM are reported. Both voltammograms are characterized by the presence of one anodic (A) and cathodic peak (A′) which are related to the Fe^{3+}/Fe^{2+} redox couple. However, the peaks of the 1st cycle are broad and separated, while those of the 4th cycle are sharper and closer. This behavior suggests the activation of the electrode, due to its progressive wetting by the electrolyte.

Figure 3b compares the 4th CV cycle of LFP_PVdF_CNM and LFP_PVdF_CB. In both cases, the CV patterns present an anodic peak at ≈3.6 V versus Li^+/Li (A), which can be assigned to the oxidation of Fe^{2+} to Fe^{3+}, and a cathodic peak at ≈3.3 V versus Li^+/Li (A′), which can be assigned to the reduction of Fe^{3+} to Fe^{2+}. However, in the case of LFP_PVdF_CNM, the oxidation peak (3.6 V vs. Li^+/Li) is at a slightly lower potential value than LFP_PVdF_CB (3.65 V vs. Li^+/Li), suggesting a lower polarization of the former cathode.

In Figure 3c, the results of the rate capability test of LFP_PVdF_CNM and LFP_PVdF_CB are reported. At C/10, both electrodes show similar electrochemical performance, with specific capacity values near 150 mAh g^{-1}. However, at higher C-rates (from C/5 up to 1C), the electrode made with CB features slightly better performance in terms of specific capacity. Furthermore, even in the final C/5 cycles, LFP_PVdF_CB exhibits slightly higher specific capacity than LFP_PVdF_CNM.

Figure 4 reports the main results of the voltammetric and galvanostatic characterization of LFP electrodes produced with Na_Alg and CNM or CB. Even in the case of LFP_Alg_CNM (Figure 4a), the 1st CV cycle is characterized by broad and separated peaks, while upon cycling (see the 4th CV cycle) the peaks become sharper and closer. As mentioned above, this behavior strongly suggests a progressive wetting of the electrode by the electrolyte upon cycling. No other signal different from that related to the Fe^{3+}/Fe^{2+} redox couple is present. Figure 4b

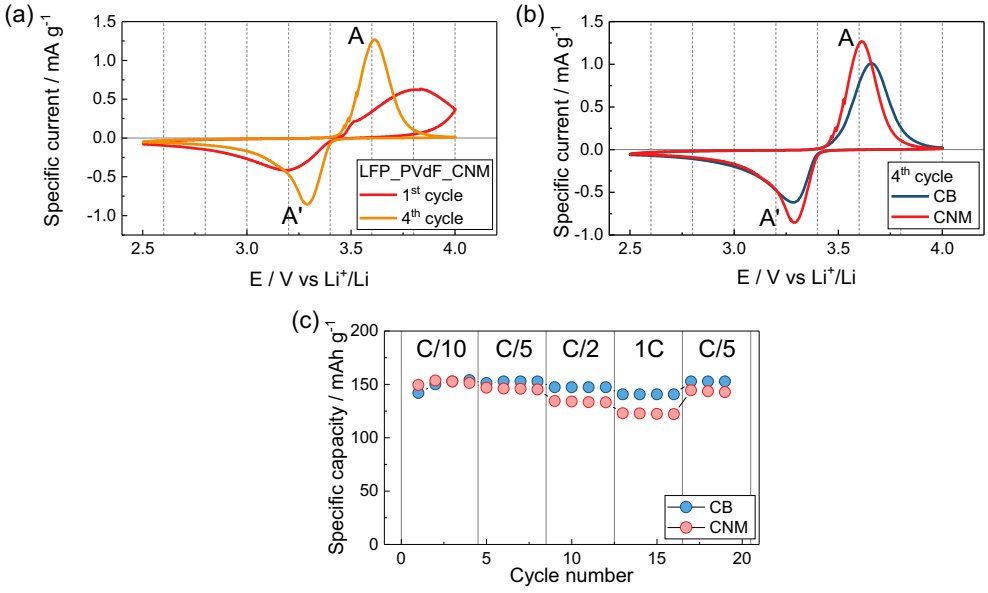

Figure 3. a) 1st and 4th CV cycles of LFP_PVdF_CNM electrode. b) Comparison of the 4th CV cycle of LFP_PVdF_CB and LFP_PVdF_CNM ($\nu = 200\ \mu V\ s^{-1}$, electrode potential range 2.5 V/4.0 V vs. Li^+/Li). c) Comparison of the rate capability of LFP_PVdF_CB and LFP_PVdF_CNM (four cycles at C/10, four cycles at C/5, four cycles at C/2, four cycles at 1C, and three cycles at C/5, electrode potential range 2.5 V/4.0 V vs. Li^+/Li).

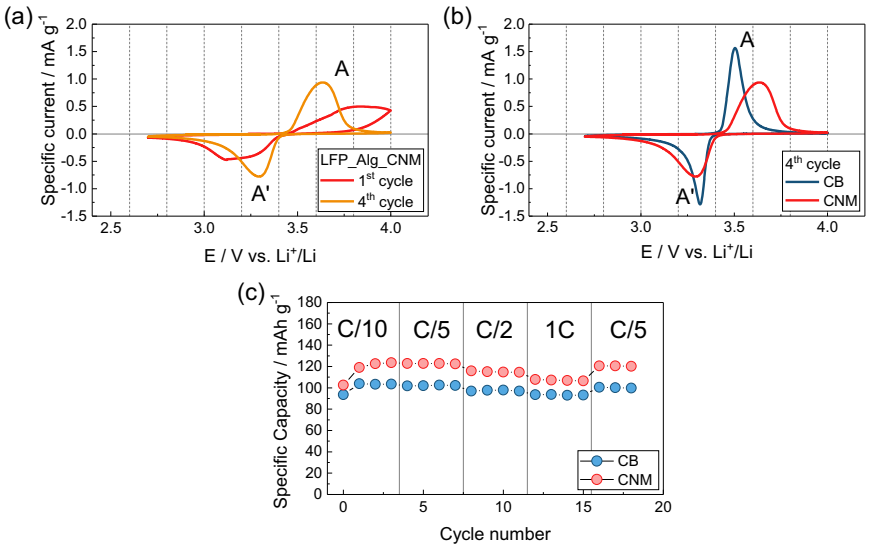

Figure 4. a) 1st and 4th CV cycles of LFP_Alg_CNM electrode. b) Comparison of the 4th CV cycle of LFP_Alg_CB and LFP_Alg_CNM ($\nu = 200\ \mu V\ s^{-1}$, electrode potential range 2.5 V/4.0 V vs. Li^+/Li). c) Comparison of the rate capability of LFP_Alg_CB and LFP_Alg_CNM (four cycles at C/10, four cycles at C/5, four cycles at C/2, four cycles at 1C, and three cycles at C/5, electrode potential range 2.5 V/4.0 V vs. Li^+/Li).

compares the 4th CV cycle of both LFP_Alg_CNM and LFP_Alg_CB. In the case of CB-based electrodes, sharper CV anodic and cathodic peaks can be observed at 3.5 V versus Li^+/Li and 3.3 V versus Li^+/Li, respectively. The CV peaks of CNM-based electrode are broader and centered at 3.6 V versus Li^+/Li and 3.3 V versus Li^+/Li, suggesting a possible poor electronic contact between LFP and CNM, and LFP and the current collector. However, as shown in Figure 4c, this behavior does not necessarily mean that CNM-based electrodes have poor electrochemical performance. Indeed, in the rate capability test, the LFP_Alg_CNM electrode was able to deliver higher specific capacities than LFP_Alg_CB, in all the applied current rates.

3.2.2. Characterization of Graphite-Based Electrodes

Figure 5 reports the main results of the voltametric and galvanostatic characterization of graphite electrodes produced with pVDF and CNM or CB. Figure 5a compares the 1st and 4th CV cycle of the G_PVdF_CNM electrode. During the first voltammetric cathodic scan (two reduction peaks can be identified. The signal at 0.55 V versus Li^+/Li is ascribed to the decomposition of the electrolyte toward the surface of the electrode and formation of the solid–electrolyte interphase (SEI).[37] The peak at 0.13 V versus Li^+/Li represents the intercalation of Li^+ ions into the graphite scaffold. During the anodic peak at 0.3 V versus Li^+/Li is due to the deintercalation of Li^+ ions from the graphite crystalline lattice. In the 4th cycle, the CV pattern is preserved except for the reduction peak due to the electrolyte decomposition, suggesting a stable formation of the SEI layer.

Figure 5b compares the 4th CV cycle of G_PVdF_CB and G_PVdF_CNM. In both cases, the CV shape is representative of graphite lithiation/delithiation. Both electrodes present a similar current response; however, in the case of the CB-based electrode, sharper peaks were observed, suggesting a better carbon–graphite-current collector connection. In Figure 5c, the rate capability tests of both electrodes are reported. At C/20, in the case of G_PVdF_CNM, specific capacity increases over cycling, suggesting a possible activation of the electrodes due to the wetting by the electrolyte. From C/10 up to C/2, both electrodes reach almost the theoretical specific capacity of graphite (i.e., 372 mAh g^{-1}), with the CNM-based electrode performance being slightly lower specific capacity than CB-based electrode. A large decrease of the specific capacity was observed in both electrodes at 1C. This behavior can be addressed to the graphite specimen used in this work (SFG44), which may not have the tailored physicochemical properties for high-C-rate application.

Figure 6 reports the electrochemical results of the graphite electrodes produced with Na–alginate and CNM or CB. As for the electrodes processed with pVdF (Figure 5a), the 1st CV pattern (Figure 6a) is characterized by a cathodic peak at 0.6 V versus Li^+/Li due to the SEI formation, followed by the main peak related to the intercalation of Li^+ ions into graphite. In the 4th cycle, the CV pattern is retained without the peak due to electrolyte decomposition, proving the formation of a stable SEI layer. Figure 6b, compares the 4th CV cycle of CB- and CNM-based electrodes. In both cases, the CV patterns are representative of the graphite lithiation/delithiation and no particular differences in the peaks position can be observed. However, the peaks of the CB-based electrode are sharper, suggesting a better electronic connection between CB–graphite-current collector. However, the G_Alg_CNM electrode was able to deliver a higher specific capacity at C/20, C10, and C/5 in the rate capability test (Figure 6c). As observed in Figure 5c, a decrease of the specific capacity was observed at 1C and can be assigned to the physicochemical properties of SFG44 not suitable for high-C-rate cycling.

Figure 7 compares the cycling stability of the LFP and graphite electrodes formulated with the different carbons and Na–Alg binder. Figure 7a shows the comparison of LFP electrodes with

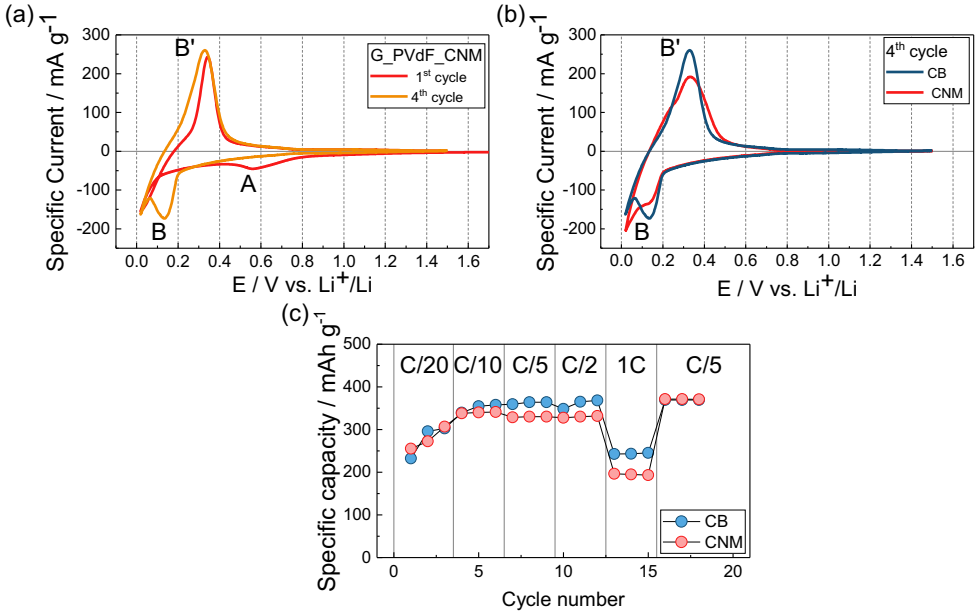

Figure 5. a) 1st and 4th CV cycles of G_PVdF_CNM electrode. b) Comparison of the 4th CV cycle of G_PVdF_CB and G_PVdF_CNM ($\nu = 200\ \mu V\ s^{-1}$, electrode potential range 0.01 V/1.5 V vs. Li^+/Li). c) Comparison of the rate capability of G_PVdF_CB and G_PVdF_CNM (three cycles at C/20, three cycles at C/10, three cycles at C/5, three cycles at C/2, three cycles at 1C, and three cycles at C/5, electrode potential range 0.01 V/1.5 V vs. Li^+/Li).

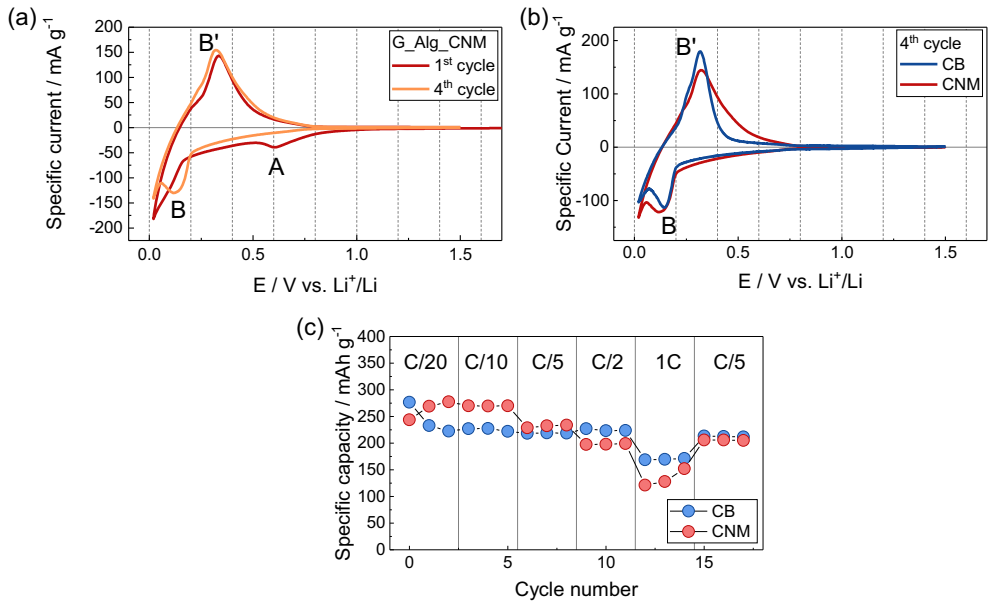

Figure 6. a) 1st and 4th CV cycles of G_Alg_CNM electrode. b) Comparison of the 4th CV cycle of G_Alg_CB and G_Alg_CNM ($\nu = 200\ \mu V\ s^{-1}$, electrode potential range 0.01 V/1.5 V vs. Li^+/Li). c) Comparison of the rate capability of G_Alg_CB and G_Alg_CNM (three cycles at C/20, three cycles at C/10, three cycles at C/5, three cycles at C/2, three cycles at 1C, and three cycles at C/5; electrode potential range 0.01 V/1.5 V vs. Li^+/Li).

alginate and CNM or CB as conductive additives. Figure 7b reports the cycling behavior of the graphite electrodes produced with Na_Alg and CNM or CB. It is clear that the substitution of CB with the greener CNM alternative bring about both LFP and graphite electrodes that feature the same electrochemical performance and stability over cycling than their homologues with CB. Indeed, the electrochemical performance observed with the electrodes prepared with water-processable binder and carbon from CO_2 electrochemical reduction is completely similar to the benchmark electrodes with a capacity retention >98% at the 100th cycle.

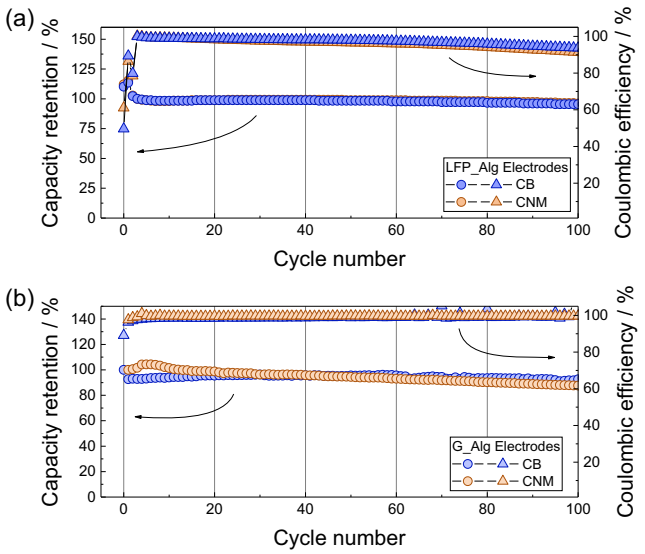

Figure 7. Capacity retention over cycling at 1C of a) LFP_Alg_CB and LFP_Alg_CNM (171 mA g^{-1} 2.5 and 4.0 V vs. Li^+/Li and b) G_Alg_CB and G_Alg_CNM (372 mA g^{-1} between 0.01 and 1.5 V vs. Li^+/Li).

4. Conclusion

Electrochemically utilized CO_2 in a molten electrolyte proves to be an attractive method of producing CNM sustainably. The use of such CNMs as additive in LIB electrodes was here explored as a sustainable raw material alternative to conventional CB. Substitution of CB with CNM, both in conventional electrode formulations featuring PVdF binder or greener versions with water-processable Na–Alg, provided similar performance. However, at the highest C-rates, CB seems to provide better capacity retention, presumably for a better electronic connection provided by the CB nanoparticles. Thus, the use of CNMs as electronic conductive additive not only decreases the CO_2 footprint impact by substituting CB but also produces good performing electrodes with greener and cheaper manufacturing, especially using water-based slurries.

As the improvement of electric conductivity directly depends on the distribution of CNMs in the electrode, additional studies for improved dispersion of CNMs in the electrode manufacturing process can help to uncover additional potential as their use as conductive material. As changes in the electrode mixing procedure can yield relevant impacts on the dispersion of CNMs in the electrode slurry,[38] procedures for materials with aspect ratios significantly different than 1 most probably have to be adjusted for optimal results in distribution. Furthermore, the impact of the CNM's aspect ratio (width/length) on the final electrode's electrical conductivity should be studied in the future by CNMs with different lengths and widths.

Acknowledgements

This work was supported by the project CO2CARBON, Upscaling carbon nanomaterial production from CO_2 emissions (KAVA Call 8, 01.01.2022–31.12.2023, funded by the European Union, EU). This study was carried out within the MOST e Sustainable Mobility Center and received funding from the European Union Next-GenerationEU (PIANO NAZIONALE DI RIPRESA E RESILIENZA (PNRR) e MISSIONE 4 COMPONENTE 2, INVESTIMENTO 1.4 e D.D. 1033 17/06/2022, CN00000023). This manuscript reflects only the authors' views and opinions, neither the European Union nor the European Commission can be considered responsible for them.

Conflict of Interest

The authors declare no conflict of interest.

Author Contributions

Nicolò Albanelli: data curation (equal); formal analysis (equal); validation (equal). **Alessandro Gregucci**: data curation (equal); investigation (equal). **Shoayb Mojtahedi**: data curation (equal); investigation (equal). **Antunes Staffolani**: formal analysis (equal); visualization (equal); writing—original draft (lead); writing—review & editing (equal). **Sander Ratso**: methodology (equal); resources (equal); writing—review & editing (equal). **Einar Karu**: investigation (equal); resources (equal); supervision (equal); writing—review & editing (equal). **Sebastian Pohlmann**: conceptualization (equal); data curation (equal); resources (equal); visualization (equal). **Catia Arbizzani**: conceptualization (equal); funding acquisition (equal); supervision (equal); writing—review & editing (equal). **Francesca Soavi**: conceptualization (lead); methodology (equal); resources (equal); supervision (equal); writing—review & editing (equal).

Data Availability Statement

The data that support the findings of this study are available from the corresponding author upon reasonable request.

Keywords

carbon nanomaterials, carbon nanotubes, CO_2 capture, CO_2 utilization, Li-ion batteries

Received: February 12, 2025
Revised: March 27, 2025
Published online:

[1] C. Tebaldi, R. Ranasinghe, M. Vousdoukas, D. J. Rasmussen, B. Vega-Westhoff, E. Kirezci, R. E. Kopp, R. Sriver, L. Mentaschi, *Nat. Clim. Change* **2021**, *11*, 746.
[2] J. Chen, S. Kang, Q. You, Y. Zhang, W. Du, *Anthropocene* **2022**, *40*, 100349.
[3] J. Huang, G. Zhang, Y. Zhang, X. Guan, Y. Wei, R. Guo, *Land Degrad. Dev.* **2020**, *31*, 1380.
[4] F. Rodrigues do Nascimento, Global Environmental Change, Climate Crisis and Desertification, Global Environmental Changes, Desertification and Sustainability **2023**, p. 9.
[5] G. Myhre, K. Alterskjær, C. W. Stjern, Ø. Hodnebrog, L. Marelle, B. H. Samset, J. Sillmann, N. Schaller, E. Fischer, M. Schulz, A. Stohl, *Sci. Rep.* **2019**, *9*, 16063.
[6] D. I. A. McKay, A. Staal, J. F. Abrams, R. Winkelmann, B. Sakschewski, S. Loriani, I. Fetzer, S. E. Cornell, J. Rockström, T. M. Lenton, *Science* **2022**, *377*, 7950.
[7] U.S. Environmental Protection Agency, *Climate Change Indicators in the United States* (Fifth Ed., EPA 430-R-24-003) **2024**.

[8] W. F. Lamb, T. Wiedmann, J. Pongratz, R. Andrew, M. Crippa, J. G. J. Olivier, D. Wiedenhofer, G. Mattioli, A. Al Khourdajie, J. House, S. Pachauri, M. Figueroa, Y. Saheb, R. Slade, K. Hubacek, L. Sun, S. K. Ribeiro, S. Khennas, S. De La Rue Du Can, L. Chapungu, S. J. Davis, I. Bashmakov, H. Dai, S. Dhakal, X. Tan, Y. Geng, B. Gu, J. Minx, *Environ. Res. Lett.* **2021**, *16*, 073005.
[9] K. O. Yoro, M. O. Daramola, *Advanced Carbon Capture Methods: Technologies and Applications*, Woodhead Publishing **2020**, p. 3.
[10] B. Scrosati, J. Garche, *J. Power Sources* **2010**, *195*, 2419.
[11] U.S. Environmental Protection Agency, *Compilation of Air Emissions Factors* **2024**, pp. 6.1-1–6.1-10.
[12] T. H. Lin, Y. S. Chien, W. M. Chiu, *Int. J. Green Energy* **2017**, *14*, 97.
[13] Y. Liang, J. Su, B. Xi, Y. Yu, D. Ji, Y. Sun, C. Cui, J. Zhu, *Resour. Conserv. Recycl.* **2017**, *117*, 285.
[14] J. Sadhukhan, M. Christensen, *Energies* **2021**, *14*, 5555.
[15] J. Ren, M. Johnson, R. Singhal, J. Licht, *J. CO2 Util.* **2017**, *18*, 335.
[16] G. Lacarbonara, S. Chini, S. Ratso, I. Kruusenberg, C. Arbizzani, *Mater. Adv.* **2022**, *3*, 7087.
[17] J. Ren, F. F. Li, J. Lau, L. González-Urbina, S. Licht, *Nano Lett.* **2015**, *15*, 6142.
[18] S. Ratso, P. R. Walke, V. Mikli, J. Ločs, K. Šmits, V. Vītola, A. Šutka, I. Kruusenberg, *Green Chem.* **2021**, *23*, 4435.
[19] M. Ramdin, B. De Mot, A. R. T. Morrison, T. Breugelmans, L. J. P. Van Den Broeke, J. P. M. Trusler, R. Kortlever, W. De Jong, O. A. Moultos, P. Xiao, P. A. Webley, T. J. H. Vlugt, *Ind. Eng. Chem. Res.* **2021**, *60*, 17862.
[20] V. Kaplan, E. Wachtel, K. Gartsman, Y. Feldman, I. Lubomirsky, *J. Electrochem. Soc.* **2010**, *157*, B552.
[21] P. Srinivasan, P. Srinivasan, PhDT **2018**.
[22] J. Lau, G. Dey, S. Licht, *Energy Convers. Manage.* **2016**, *122*, 400.
[23] Z. Zhou, L. Ci, L. Song, X. Yan, D. Liu, H. Yuan, Y. Gao, J. Wang, L. Liu, W. Zhou, G. Wang, S. Xie, *Carbon* **2003**, *41*, 2607.
[24] N. Gupta, S. M. Gupta, S. K. Sharma, *Carbon Lett.* **2019**, *29*, 419.
[25] European Commission, *REACH*, Brussels **2019**.
[26] D. Bresser, D. Buchholz, A. Moretti, A. Varzi, S. Passerini, *Energy Environ. Sci.* **2018**, *11*, 3096.
[27] D. L. Wood, J. D. Quass, J. Li, S. Ahmed, D. Ventola, C. Daniel, *Drying Technol.* **2018**, *36*, 234.
[28] J. Li, Y. Lu, T. Yang, D. Ge, D. L. Wood, Z. Li, *iScience* **2020**, *23*, 101081.
[29] N. Lingappan, L. Kong, M. Pecht, *Renewable Sustainable Energy Rev.* **2021**, *147*, 111227.
[30] F. Bigoni, F. De Giorgio, F. Soavi, C. Arbizzani, *J. Electrochem. Soc.* **2017**, *164*, A6171.
[31] A. Brilloni, F. Poli, G. E. Spina, C. Samorì, E. Guidi, C. Gualandi, M. Maisuradze, M. Giorgetti, F. Soavi, *Electrochim. Acta* **2022**, *418*, 140376.
[32] A. Brilloni, F. Marchesini, F. Poli, E. Petri, F. Soavi, *Energies* **2022**, *15*, 2608.
[33] I. Kruusenberg, N. Alexeyeva, K. Tammeveski, J. Kozlova, L. Matisen, V. Sammelselg, J. Solla-Gullón, J. M. Feliu, *Carbon* **2011**, *49*, 4031.
[34] R. Jiang, M. Gao, X. Mao, D. Wang, *Curr. Opin. Electrochem.* **2019**, *17*, 38.
[35] T. A. Saleh, *Interface Sci. Technol.* **2022**, *34*, 99.
[36] S. Trano, D. Versaci, M. Castellino, M. Fontana, L. Fagiolari, C. Francia, F. Bella, *Energy Mater.* **2024**, *4*, 400008.
[37] E. Peled, S. Menkin, *J. Electrochem. Soc.* **2017**, *164*, A1703.
[38] W. Bauer, D. Nötzel, V. Wenzel, H. Nirschl, *J. Power Sources* **2015**, *288*, 359.